

Non-linear QCD meets data: A global analysis of lepton-proton scattering with running coupling BK evolution

Javier L. Albacete¹, Néstor Armesto², José Guilherme Milhano³ and Carlos A. Salgado²

¹ *European Center for Theoretical Studies in Nuclear Physics and Related Areas (ECT*), Strada delle Tabarelle 286, I-38050 Villazzano (TN), Italy*

² *Departamento de Física de Partículas and IGFAE, Universidade de Santiago de Compostela, E-15706 Santiago de Compostela, Spain*

³ *CENTRA, Instituto Superior Técnico (IST), Av. Rovisco Pais, P-1049-001 Lisboa, Portugal*

E-mail addresses: albacete@ect.it, nestor.armesto@usc.es, guilherme.milhano@ist.utl.pt, carlos.salgado@usc.es.

ABSTRACT: We perform a global fit to the structure function F_2 measured in lepton-proton experiments at small values of Bjorken- x , $x \leq 0.01$, for all experimentally available values of Q^2 , $0.045 \text{ GeV}^2 \leq Q^2 \leq 800 \text{ GeV}^2$. We show that the recent improvements resulting from the inclusion of running coupling corrections allow for a description of data in terms of non-linear QCD evolution equations. In this approach F_2 is calculated within the dipole model with all Bjorken- x dependence described by the running coupling Balitsky-Kovchegov equation. Two different initial conditions for the evolution are used, both yielding good fits to data with $\chi^2/\text{d.o.f.} < 1.1$. Data for the proton longitudinal structure function F_L , not included in the fits, are also well described. Our analysis allows to perform a first principle extrapolation of the proton-dipole scattering amplitude. We provide predictions for F_2 and F_L in the kinematical regions of interest for future colliders and ultra-high energy cosmic rays. A numerical implementation of our results down to $x = 10^{-12}$ is released as a computer code for public use.

KEYWORDS: High-energy QCD, lepton-hadron collisions, dipole model, non-linear QCD evolution.

Contents

1. Introduction	1
2. Setup	5
2.1 Dipole model	5
2.2 BK equation with running coupling	6
2.3 Regularization of the infrared dynamics	9
2.4 Initial conditions for the evolution	10
2.5 Summary of the theoretical setup and free parameters	11
3. Numerical method and experimental data	11
4. Results	12
4.1 Fits to F_2 and description of F_L	12
4.2 Predictions for future experimental programs	15
4.3 Parametrizations of the dipole-proton scattering amplitude	17
5. Conclusions	17

1. Introduction

The experimental data collected in electron-proton deep inelastic scattering (DIS) experiments [1–18] at small values of Bjorken- x constitute one of the most valuable sources of information to test and explore the high-energy limit of Quantum Chromodynamics (QCD). The standard analyses (see [19] and references therein) of these data are usually made in the framework of fixed order DGLAP evolution equations in which various resummation schemes have also been essayed. On the other hand a description of available data in terms of the non-linear QCD evolution equations [20–27] has — despite phenomenological analyses (see e.g. [28–34]) being most suggestive of the presence of *saturation* effects, a crucial physical ingredient for the description of high-energy scattering in the small- x domain of DIS — been elusive so far.

The saturation phenomenon is closely related to unitarity of the quantum field theory and is characteristic of dense partonic systems. It admits an intuitively clear physical picture in the infinite momentum frame. There, the gluon distribution function $xG(x, Q^2)$ can be interpreted as the number of gluons in the proton wave function

localized within a transverse area inversely proportional to the photon virtuality Q^2 , and carrying a fraction of the proton longitudinal momentum x . For fixed Q^2 , the number of gluons in the proton wave function increases with decreasing x due to additional gluon emission or gluon branching. Such growth of gluon densities has been experimentally observed at HERA and, if extrapolated towards smaller values of x , would threaten the unitarity of the theory. Hence, the proton gets denser and gluon-gluon recombination processes, which are essentially non-linear, slow down the non-abelian avalanche towards small- x . This mechanism tames the subsequent growth of gluon densities, i.e. they *saturate*, thus preventing unitarity violations. The intrinsic momentum scale that determines the separation between the dilute and dense domains in the proton wave function is the saturation scale $Q_s^2(x)$. This scale can be understood as the inverse transverse area inside which the probability of finding more than one gluon is of order one. It is a dynamic scale whose growth is determined by the interplay between the linear, radiative processes and the non-linear, recombination ones.

All these qualitative ideas are cast in a definite theoretical framework, the Color Glass Condensate (CGC). The CGC is endowed with a set of perturbative, non-linear evolution equations, the Jalilian-Marian–Iancu–McLerran–Weigert–Leonidov–Kovner (JIMWLK) equation [20–25] and the Balitsky-Kovchegov (BK) equation [26, 27], that describe the small- x evolution of hadronic wave functions. However, rather than in terms of partonic densities, high-energy QCD evolution is more naturally formulated in terms of correlators of Wilson lines as effective degrees of freedom. The JIMWLK equation is equivalent to an infinite set of coupled, non-linear evolution equations for all correlators of the Wilson lines – also known as Balitsky’s hierarchy. In the limit of large number of colors (N_c) the hierarchy reduces to a single equation – the BK equation – for the correlator of two Wilson lines or, equivalently, for the (imaginary part of the) dipole scattering amplitude \mathcal{N} . As we shall explain in detail in Section 2, in the dipole model the small- x dependence of the different DIS cross sections is completely encoded in the dipole scattering amplitude, and thus describable by the JIMWLK-BK equations.

Even though the JIMWLK equation comprises a richer physical input than the BK equation, the latter has become the most widely used tool to study the small- x dynamics. This is in part due to the relative simplicity of the BK equation with respect to JIMWLK, whose solution demands the use of rather complicated numerical methods [35]. Further, the difference between the solutions of the BK and JIMWLK equations turns out to be significantly smaller, of order 0.1% [35], than the a priori expected $\mathcal{O}(1/N_c^2)$ corrections. The origin of the smallness of the subleading- N_c corrections have been investigated recently in [36]. For these reasons, here we will consider the BK equation, rather than JIMWLK, as the starting point to analyse the experimental data on the proton structure functions at small- x .

One of the first and most successful phenomenological applications of satura-

tion based ideas to the description of small- x DIS data is due to Golec-Biernat and Wüsthoff (GBW) [28]. Their pioneering work relies on the use of the dipole model in QCD [37,38], together with a relatively simple model for the dipole-proton scattering amplitude encoding the basic features of saturation, to calculate the DIS total and diffractive lepton-proton cross sections. In particular, the proton saturation scale was parametrized as $Q_s^2(x) = (x_0/x)^\lambda \text{ GeV}^2$. Fits to HERA data yielded $x_0 = 3 \cdot 10^{-4}$ and $\lambda = 0.288$. Several improvements of the GBW model for the dipole scattering amplitude were proposed later on in [29,31–34,39]. Very succinctly, some of these works [29] incorporated features of BFKL dynamics and explicit impact parameter dependence in the scattering amplitude [30,32,33], whereas [39] focused in including DGLAP evolution into the model, which resulted in a improved fit to the higher Q^2 data. A first attempt of combining BK and DGLAP dynamics in the description of DIS data was made in [30]. Finally, the relation to heavy ion collisions was explored in [31,34]. Overall, these works reported an evolution speed compatible with the one obtained in the GBW model, $\lambda \sim 0.2 \div 0.3$.

A natural question arises of why the BK-JIMWLK equations, the most solid theoretical tool available to describe the small- x dynamics of the dipole scattering amplitude and, in particular, the x -dependence of the saturation scale, have not been directly applied to the study of DIS small- x data. The answer to this question is given by the analytical [40,41] and numerical [42–44] studies of the leading-order (LO) BK equation. In these works the growth of the saturation scale yielded by the LO BK equation was determined to be $Q_s^2 \sim x^{-\lambda_{LO}}$, with $\lambda_{LO} \simeq 4.88 N_c \alpha_s / \pi$. Thus, the LO result predicts a much faster growth of the saturation scale (and hence of DIS structure functions) with decreasing x than the one extracted phenomenologically. This insufficiency of LO BK can only be circumvented by introducing an unreasonably small value for the fixed coupling, rendering any attempt to describe experimental data far from meaningful.

It has been a long-standing expectation that higher order corrections to the original LO BK-JIMWLK equations could bring the theoretical predictions closer to experimental observations. Indeed, numerical estimates for the running coupling [43,44] and energy conservation corrections [44,45] – both subleading physical contributions to the LO kernel – based on heuristic modifications of the LO kernel indicated a significant reduction of the evolution speed, thus pointing in the right direction. Moreover, running coupling effects appeared to dominate the contribution to the evolution kernel with respect to energy conservation effects [44]. However, it was not until recently that an explicit first principle calculation of the running coupling corrections to the evolution kernel was performed in [46–48] by including $\alpha_s N_f$ corrections (N_f being the number of flavors) into the evolution kernel to all orders and by then completing N_f to the one-loop QCD beta-function. The numerical study of the BK equation at all orders in $\alpha_s N_f$, performed in [49], reported a significant slowdown of the evolution speed with respect to the solutions of the LO equation, hence

rising the hopes that the improved equation might become a useful phenomenological tool. In its first successful application it was used to describe the energy and rapidity dependences of particle multiplicities produced in nucleus-nucleus collisions at the Relativistic Heavy Ion Collider (RHIC) at the BNL [50].

Significant progress has also been made recently in the determination of subleading physical effects, other than running coupling corrections, to the LO BK equation, namely the inclusion of pomeron loops (see e.g. [51,52] and references therein), finite- N_c corrections [36] or the determination of the complete next-to-leading evolution kernel [53] to the BK equation. However, our current understanding indicates that the running coupling effects are dominant with respect to pomeron loops (or particle number fluctuations) [54] or finite N_c corrections [36]. We will therefore limit ourselves in the present work to the analysis of DIS small- x data via the BK equation including *only* running coupling corrections.

The first goal of this paper is to prove the ability of the BK equation including running coupling corrections to account for the small- x behavior of the total, F_2 , and longitudinal, F_L , structure functions measured in DIS experiments (a first step in this direction, yet unpublished, was reported in [55]). To that end we shall devise a global fit to the available experimental data with $x \leq x_0 = 10^{-2}$ and for all values of Q^2 . Analogously to previous works, our starting point will be the dipole model of QCD. The main novelty of our work is that the dipole-proton scattering amplitude, instead of being modeled, is calculated via numerical solutions of the BK equation including running coupling corrections. The free parameters in our fit, to be detailed in Section 2, are those related to the parametrization of the initial condition for the evolution, a global coefficient that sets the normalization and a constant which relates the running of the coupling in momentum space to that in dipole size. As we show in Section 4.1, the fits yield a good $\chi^2/\text{d.o.f.} \leq 1.1$, thus demonstrating that such partial improvement of the LO BK equation suffices to reconcile the theoretical predictions with experimental results. Further, in Section 4.2 with all the free parameters fixed by the global fit of available data, we make predictions for the same observables at much smaller values of x . Such predictions are completely driven by non-linear QCD dynamics and could be directly tested at the proposed Electron-Ion Collider (EIC) [56] or Large Hadron-electron Collider (LHeC) [57] experimental facilities, where values of x as low as $x \sim 10^{-7}$ for $Q^2 \sim 1 \text{ GeV}^2$ could be reached.

Second, the upcoming LHC experimental programs in proton-proton, proton-nucleus and nucleus-nucleus demand a detailed knowledge of hadronic wave functions or parton density functions (PDF) at very small x as an input for the calculation of many different observables (see, for instance, the discussions in [19, 58]). While global PDF fits provide a description of currently available data, additional theoretical input is needed in order to safely extrapolate towards values of x so far unexplored empirically and for which additional saturation effects appear unavoidable. A similar situation is found in cosmic rays physics [59, 60], where the highest

center-of-mass energies reached in primary collisions are simply unattainable in accelerator experiments in the foreseeable future. In this work we set the ground for a systematic program oriented to provide parameter-free extrapolations of the dipole amplitudes (both for proton and nuclei) to very small values of x based on first principle calculations. Parametrizations of the dipole-proton scattering amplitudes down to very small x based on the results of this work are publicly available through simple numeric routines [61].

2. Setup

In this section we briefly review, in a self contained manner, the main ingredients needed for the calculation of the inclusive and longitudinal DIS structure functions.

2.1 Dipole model

At $x \ll 1$, the inclusive structure function of DIS can be expressed as

$$F_2(x, Q^2) = \frac{Q^2}{4\pi^2\alpha_{em}} (\sigma_T + \sigma_L), \quad (2.1)$$

where α_{em} is the electromagnetic coupling and $\sigma_{T,L}$ stands for the virtual photon-proton cross section for transverse (T) and longitudinal (L) polarizations of the virtual photon. The longitudinal structure function is obtained by considering only the longitudinal contribution:

$$F_L(x, Q^2) = \frac{Q^2}{4\pi^2\alpha_{em}} \sigma_L. \quad (2.2)$$

It is well known that at high energies or small x (where the coherence length of the virtual photon fluctuation $l_c \approx (2m_N x)^{-1} \simeq 0.1/x$ fm $\gg R_N$, with m_N and R_N the proton mass and radius respectively), and using light-cone perturbation theory, the total virtual photon-proton cross section can be written as the convolution of the light-cone wave function squared for a virtual photon to fluctuate into a quark-antiquark dipole, $|\Psi_{T,L}|^2$, and the imaginary part of the dipole-target scattering amplitude, \mathcal{N} . For transverse and longitudinal polarizations of the virtual photon one writes [37, 38]:

$$\sigma_{T,L}(x, Q^2) = \int_0^1 dz \int d\mathbf{b} d\mathbf{r} |\Psi_{T,L}(z, Q^2, \mathbf{r})|^2 \mathcal{N}(\mathbf{b}, \mathbf{r}, x), \quad (2.3)$$

where z is the fraction of longitudinal momentum of the photon carried by the quark, \mathbf{r} is the transverse separation between the quark and the antiquark and \mathbf{b} the impact parameter of the dipole-target collision (henceforth boldface notation indicates two-dimensional vectors). The wave functions $|\Psi_{T,L}|^2$ for the splitting of the photon into a $q\bar{q}$ dipole are perturbatively computable within QED. We refer the

reader to e.g. [28] for explicit expressions to lowest order in α_{em} . All the information about the strong interactions – along with all x -dependence – in Eq. (2.3) is encoded in the dipole-proton scattering amplitude, $\mathcal{N}(\mathbf{b}, \mathbf{r}, x)$. Although this quantity is a genuinely non-perturbative object, its evolution towards smaller values of x can be studied perturbatively via the BK equation. On the contrary, its impact parameter dependence cannot be studied by means of the perturbative BK equation, since it is governed by long distance, non-perturbative physics. To circumvent this theoretical limitation we will resort to the translational invariance approximation (also used in [28]), which regards the proton as homogeneous in the transverse plane. Under this approximation the virtual photon-proton cross section Eq. (2.3) can be rewritten as follows:

$$\sigma_{T,L}(x, Q^2) = \sigma_0 \int_0^1 dz \int d\mathbf{r} |\Psi_{T,L}(z, Q^2, \mathbf{r})|^2 \mathcal{N}(r, Y), \quad (2.4)$$

where $r = |\mathbf{r}|$ is the dipole size (the notation $v \equiv |\mathbf{v}|$ for all the 2-dimensional vectors will be also employed throughout the rest of the paper) and σ_0 is a dimensionful constant resulting from the \mathbf{b} integration that sets the normalization – this will be one of the free parameters in our fits. Note that this result relies on the assumption that a factorized structure of x, r and b dependences remains unchanged throughout the evolution. In this case the parameter σ_0 is related to the t -dependence in diffractive events, see e.g. [62]. On the other hand, this factorized structure may be assumed solely for the initial condition, while small- x evolution is performed, in the translational-invariant approximation, separately for every impact parameter (as done e.g. for nuclei in [63, 64]). This results in a σ_0 varying (increasing) with energy [65]. We leave this latter aspect for future studies.

2.2 BK equation with running coupling

The primary physical mechanism driving the small- x evolution of the dipole scattering amplitude is the emission of soft gluons off either the quark or the antiquark in the original dipole. The leading order BK equation resumming the corresponding $\alpha_s \ln(1/x)$ contributions to all orders reads

$$\begin{aligned} \frac{\partial \mathcal{N}(r, Y)}{\partial Y} &= \int d\mathbf{r}_1 K^{\text{LO}}(\mathbf{r}, \mathbf{r}_1, \mathbf{r}_2) \\ &\times [\mathcal{N}(r_1, Y) + \mathcal{N}(r_2, Y) - \mathcal{N}(r, Y) - \mathcal{N}(r_1, Y)\mathcal{N}(r_2, Y)], \end{aligned} \quad (2.5)$$

with the evolution kernel given by

$$K^{\text{LO}}(\mathbf{r}, \mathbf{r}_1, \mathbf{r}_2) = \frac{N_c \alpha_s}{2\pi^2} \frac{r^2}{r_1^2 r_2^2}, \quad (2.6)$$

and $\mathbf{r}_2 = \mathbf{r} - \mathbf{r}_1$. Here, $Y = \ln(x_0/x)$ is the rapidity variable and x_0 is the value of x where the evolution starts, which should be small enough for the dipole model to be

applicable. In our case $x_0 = 0.01$ will be the highest experimental value of x included in the fit.

The calculations in [46, 47] proceeded by including $\alpha_s N_f$ corrections (N_f being the number of flavors) into the evolution kernel to all orders and by then completing N_f to the one-loop QCD beta-function via replacing $N_f \rightarrow -6\pi\beta_2$, with $\beta_2 = (11N_c - 2N_f)/(12\pi)$. The calculation of the $\alpha_s N_f$ corrections is particularly simple in the s -channel light-cone perturbation theory (LCPT) formalism used to derive the BK and JIMWLK equations: there $\alpha_s N_f$ corrections are solely due to chains of quark bubbles placed onto the s -channel gluon lines, as sketched in Fig. 1A. Importantly, at the same degree of accuracy a new physical channel is opened, namely the emission of a quark-antiquark pair, instead of a gluon, as depicted in Fig. 1B. The calculation in [48] relied instead on the use of dispersive methods, arriving at the same results as in the perturbative calculation in [47].

Neglecting the impact parameter dependence, the improved BK evolution equation for the dipole scattering amplitude obtained after resumming the subleading $\alpha_s N_f$ corrections to all orders in [46, 47] can be written in the following, rather general form [49]:

$$\frac{\partial \mathcal{N}(r, Y)}{\partial Y} = \mathcal{R}[\mathcal{N}] - \mathcal{S}[\mathcal{N}], \quad (2.7)$$

where both \mathcal{R} and \mathcal{S} are functionals of the dipole scattering amplitude, \mathcal{N} . The first, *running coupling*, term $\mathcal{R}[\mathcal{N}]$ in Eq. (2.7) gathers all the $\alpha_s N_f$ factors needed to complete the QCD beta function, resulting in a functional form identical to the LO one but involving a modified kernel which provides the scale setting for the running of the coupling. In turn, the second term in the r.h.s. of Eq. (2.7), $\mathcal{S}[\mathcal{N}]$, the *subtraction* term, accounts for conformal, non running-coupling contributions.

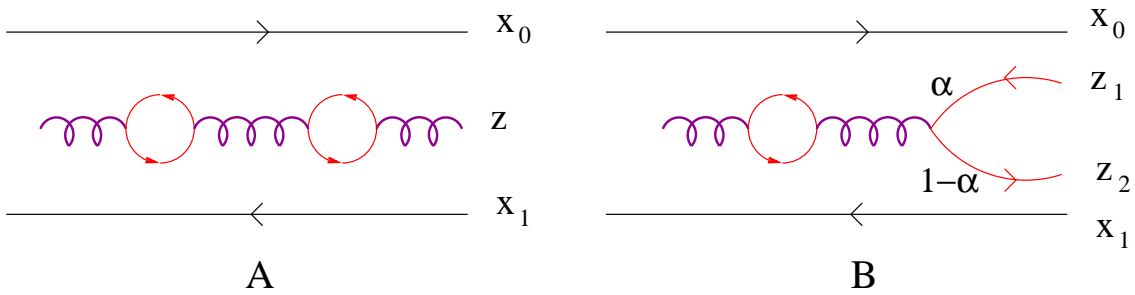


Figure 1: Schematic representation of the diagrams contributing to the evolution to all orders in $\alpha_s N_f$. The s -channel gluon line can be attached to either the quark (upper line) or the antiquark (lower line).

It would be erroneous to identify the gluon and quark-antiquark emission channels with the running and subtraction terms in Eq. (2.7) respectively. Importantly, the quark-antiquark channel contains a logarithmic ultra-violet (UV) divergence as-

sociated to the emission of a zero size pair which, in the large- N_c limit, is indistinguishable from one gluon emission and therefore contributes to the running of the coupling on an equal footing. The emission of finite size quark-antiquark pairs is UV finite and does not contribute to the running of the coupling. Thus, the decomposition of the evolution kernel into *running* and *subtraction* contributions, although constrained by unitarity arguments, is not unique. This is due to the fact that there is some freedom in the way in which the UV divergence can be singled out from the *conformal* one, so in order to perform a decomposition like the one in Eq. (2.7) a precise separation scheme needs to be specified. Not surprisingly, the separation schemes proposed in [46] and [47] were different. For a detailed discussion on this subject we refer the reader to [49].

In this work we will consider only the *running* term in the evolution kernel. Ideally one would like to include the *subtraction* piece of the evolution kernel in practical applications as this would eliminate the uncertainty associated to the scheme choice and would provide a richer physical description of the small- x evolution of the dipole scattering amplitude. Unfortunately, its numerical evaluation [49] demands a very large computing time. For a global fit like the one presented in this work, in which the evolution is performed $\sim 10^3$ times, such computing time is simply unaffordable. On the other hand, as shown in [49] the contribution to the complete evolution kernel stemming from the *subtraction* term is systematically smaller – and negligible at high rapidities – than the one arising from the *running* term. In particular, we will follow the prescription proposed by Balitsky in [46] to single out the *running* term since, as demonstrated in [49], such choice minimizes the contribution to the evolution of the *subtraction* term, neglected in what follows, with respect to the separation scheme proposed in [47].

Finally, after dropping the subtraction term from Eq. (2.7), the BK evolution equation including *only* running coupling corrections reads

$$\frac{\partial \mathcal{N}(r, Y)}{\partial Y} = \mathcal{R}^{\text{Bal}}[\mathcal{N}], \quad (2.8)$$

where the running coupling functional is identical to the LO equation:

$$\begin{aligned} \mathcal{R}^{\text{Bal}}[\mathcal{N}] &= \int d\mathbf{r}_1 K^{\text{Bal}}(\mathbf{r}, \mathbf{r}_1, \mathbf{r}_2) \\ &\times [\mathcal{N}(r_1, Y) + \mathcal{N}(r_2, Y) - \mathcal{N}(r, Y) - \mathcal{N}(r_1, Y) \mathcal{N}(r_2, Y)], \end{aligned} \quad (2.9)$$

but with a modified evolution kernel that includes running coupling corrections. Using Balitsky's prescription, the kernel for the *running* term reads [46]

$$K^{\text{Bal}}(\mathbf{r}, \mathbf{r}_1, \mathbf{r}_2) = \frac{N_c \alpha_s(r^2)}{2\pi^2} \left[\frac{r^2}{r_1^2 r_2^2} + \frac{1}{r_1^2} \left(\frac{\alpha_s(r_1^2)}{\alpha_s(r_2^2)} - 1 \right) + \frac{1}{r_2^2} \left(\frac{\alpha_s(r_2^2)}{\alpha_s(r_1^2)} - 1 \right) \right]. \quad (2.10)$$

2.3 Regularization of the infrared dynamics

The BK equation is an integro-differential equation that involves integration over all available phase-space for soft gluon emission. In the running coupling case, Eqs. (2.8-2.10), the coupling has to be evaluated at arbitrarily large values of the dipole size (small gluon momentum), and a regularization prescription to avoid the Landau pole becomes necessary. A celebrated feature of the BK equation is its ability to fix [66] the problem of infra-red diffusion characteristic of its linear counterpart, the BFKL equation. The non-linear terms in the BK equation ensure that the dynamics in the phase space region within the unitarity limit, i.e. for $r \gg 1/Q_s$, is frozen. Such feature is shared by both the LO and running coupling BK equations, since it is ultimately rooted in the non-linear combination of \mathcal{N} 's in the r.h.s. of Eq. (2.9), which is identical in both cases. Thus, if Q_s is perturbatively large, $Q_s \gg \Lambda_{QCD}$, then all the relevant dynamics takes place deep in the ultra-violet region of the phase space, $r \leq 1/Q_s$. In such scenario the details about the regularization of the running coupling in the infra-red become irrelevant for the result of the evolution.

Unfortunately, we can anticipate that such will not be the case in this work. Taking the results by Golec-Biernat and Wüsthoff [28] as a guidance, one can estimate that the proton saturation scale at the largest values of Bjorken- x to be considered in this work, $x \sim 10^{-2}$, is of the order of $Q_s^2(x=10^{-2}) \approx (3 \cdot 10^{-4}/10^{-2})^{0.288} \text{ GeV}^2 \simeq 0.36 \text{ GeV}^2$. The fits to be presented in Section 4 yield even smaller values of the initial saturation scale of the proton. Although larger than Λ_{QCD}^2 , such values for the initial scale are not large enough to avoid sensitivity to the infra-red (IR) dynamics. Actually, the detailed study of the infrared-renormalon ambiguities carried out in [48] demonstrated that the sensitivity of the solutions of the evolution equation to several different prescriptions used to regularize the coupling is relatively large even for initial saturation scales as large as $Q_s^2 \sim 1 \div 2 \text{ GeV}^2$. On the bright side, theoretical studies of the Schwinger-Dyson equations for the gluon propagator in the IR and lattice QCD results (see e.g. [67,68] and references therein) indicate that the strong coupling freezes to a constant value, α_{fr} , in the IR. Moreover, the value at which the coupling freezes has been determined to be $\alpha_{fr} \sim 0.5 \div 0.7$. While these results are somewhat controversial and yet subject to discussion in the literature, in particular the very definition of an infrared coupling, we will take them as a guidance to regularize the IR dynamics. Otherwise, our prescription can be regarded as purely phenomenological.

Thus, for small dipole sizes $r < r_{fr}$, with $\alpha_s(r_{fr}^2) \equiv \alpha_{fr} = 0.7$, we shall evaluate the running coupling according to the usual one-loop QCD expression:

$$\alpha_s(r^2) = \frac{12\pi}{(11N_c - 2N_f) \ln\left(\frac{4C^2}{r^2\Lambda_{QCD}^2}\right)}, \quad (2.11)$$

with $N_f = 3$, whereas for larger sizes, $r > r_{fr}$, we freeze the coupling to the fixed value $\alpha_{fr} = 0.7$. We take $\Lambda_{QCD} = 0.241 \text{ GeV}$, such that $\alpha_s(M_Z) = 0.1176$, with M_Z the

mass of the Z boson. The factor C^2 under the logarithm in Eq. (2.11) will be one of the free parameters in the fit. It reflects the uncertainty in the Fourier transform from momentum space, where the original calculation of $\alpha_s N_f$ corrections was performed, to coordinate space. Alternatively, we could have fixed C^2 to the value suggested in [47], $e^{-5/3-2\gamma_E}$, and chosen either Λ_{QCD} or α_{fr} as the free parameters controlling the IR dynamics. Indeed, we have checked that such choices yield equally good fits as those presented in Section 4 without changing much the value of the other free parameters. However, both α_{fr} and, specially, Λ_{QCD} , are more tightly constrained from both theoretical and phenomenological studies than C^2 .

2.4 Initial conditions for the evolution

Finally we have to specify the initial condition (i.c.) for the evolution or, equivalently, the precise shape of the proton unintegrated gluon distribution (UGD), $\phi(x, k)$, at the highest experimental value of Bjorken- x included in the fit, $x_0 = 0.01$ (which, by definition, corresponds to rapidity $Y = 0$). The UGD is related to the dipole scattering amplitude via a Fourier transform:

$$\phi(x, k) = \int \frac{d\mathbf{r}}{2\pi r^2} e^{i\mathbf{k}\cdot\mathbf{r}} \mathcal{N}(x, r). \quad (2.12)$$

This is a genuinely non-perturbative object which needs to be modeled. We will consider two different families of initial conditions. The first one is inspired in the original GBW ansatz [28] for the dipole scattering amplitude and parametrized in the following way:

$$\mathcal{N}^{GBW}(r, Y=0) = 1 - \exp \left[- \left(\frac{r^2 Q_{s0}^2}{4} \right)^\gamma \right]. \quad (2.13)$$

The second family of initial conditions [69] follows closely the McLerran-Venugopalan (MV) model:

$$\mathcal{N}^{MV}(r, Y=0) = 1 - \exp \left[- \left(\frac{r^2 Q_{s0}^2}{4} \right)^\gamma \ln \left(\frac{1}{r \Lambda_{QCD}} + e \right) \right], \quad (2.14)$$

where Q_{s0}^2 is the initial saturation scale squared in both cases.

Eqs. (2.13) and (2.14) differ with respect to the original GBW and MV models in the inclusion of an anomalous dimension, γ , which will be another of the free parameters in the fit. The GBW and MV functional forms are recovered by setting $\gamma = 1$ in Eq. (2.13) and Eq. (2.14) respectively. The anomalous dimension controls the slope of the scattering amplitude in the transition from the dilute region to the black disk region. The main difference between MV and GBW i.c. is their different UV behaviour, which is more easily appreciated in momentum space. For $\gamma = 1$ and large transverse momenta k , the UGD resulting from the MV i.c. falls off as $\phi^{MV} \sim 1/k^2$, as expected from rather general perturbative considerations, while the

GBW i.c. falls off exponentially, $\phi^{GBW} \sim \exp(-k^2/Q_s^2)$. It is well known that the solutions of the BK equation, both at LO and including higher order corrections, do not respect the relatively simple functional forms in Eq. (2.13) and Eq. (2.14). On the contrary, they can be roughly characterized by an r - and Y -dependent anomalous dimension, $\gamma(r, Y)$, with $\gamma \rightarrow 1$ for $r \rightarrow 0$. Clearly a constant value of $\gamma \neq 1$ would not respect such condition. However, the main contribution to the DIS cross section given by Eq. (2.4) originates from the region $1/Q \lesssim r \lesssim 1/Q_s$. The contribution from the dilute UV region $r < 1/Q$ is much smaller and therefore we will not consider additional refinements of the initial conditions in Eq. (2.13) and Eq. (2.14), which would come at the prize of adding new, spurious parameters into the fit. [Actually, the results of the fit shows that for the GBW i.c. the preferred value is $\gamma = 1$, so it will be fixed for this initial condition.] Finally, the constant term under the logarithm in the MV initial condition, e , has been added to regularize the exponent for large values of r .

2.5 Summary of the theoretical setup and free parameters

In summary, we will calculate the total DIS inclusive and longitudinal structure functions according to the dipole model under the translational invariant approximation Eq. (2.4). The small- x dependence is completely described by means of the BK equation including running coupling corrections, Eqs. (2.8-2.10), for which two different initial conditions GBW and MV, Eqs. (2.13) and (2.14), are considered. All in all, the free parameters to be fitted to experimental data are:

- σ_0 : The total normalization of the cross section in Eq. (2.4).
- Q_{s0}^2 : The saturation scale of the proton at the highest experimental value of Bjorken- x included in the fit, $x_0 = 10^{-2}$, in Eqs. (2.13) and (2.14).
- C^2 : The parameter relating the running of the coupling in momentum space to the one in dipole size in Eq. (2.11).
- γ : The anomalous dimension of the initial condition for the evolution in Eqs. (2.13) and (2.14). As discussed in Section 4, in some cases (GBW) γ can be fixed to 1, obtaining equally good fits to data than when it is considered a free parameter.

3. Numerical method and experimental data

The experimental data included in the fit to $F_2(x, Q^2)$ have been collected by the E665 [1] (FNAL), the NMC [2] (CERN-SPS), the H1 [3–8] (HERA) and the ZEUS [9–16] (HERA) experimental Collaborations. We have considered data for $x \leq 10^{-2}$ and for all available values of Q^2 , $0.045 \text{ GeV}^2 \leq Q^2 \leq 800 \text{ GeV}^2$.

The only published direct measurements of the longitudinal structure function $F_L(x, Q^2)$ were obtained recently by the H1 [17] and ZEUS [18] Collaborations, and they are *not* included in the fit.

All in all, 847 data points are included. Statistical and systematic uncertainties were added in quadrature, and normalization uncertainties not considered. [A more involved treatment separating uncorrelated and correlated/normalization errors could be done only at the expense of adding one more fitting parameter for each of the 17 data sets used, thus making the minimization task impossible due to CPU-time requirements.] Since the minimization algorithms require a large number of calls to the function we have implemented a parallelization of the numeric code. Finally, the BK evolution equation including running coupling corrections is solved using a Runge-Kutta method of second order with rapidity step $\Delta h_y = 0.05$, see further details in [49].

In order to smoothly go to photoproduction, we follow [28] and use the redefinition of the Bjorken variable

$$\tilde{x} = x \left(1 + \frac{4m_f^2}{Q^2} \right), \quad (3.1)$$

with $m_f = 0.14$ GeV for the three light flavors we consider in Eq. (2.4).

4. Results

4.1 Fits to F_2 and description of F_L

The values of the free parameters obtained from the fits to data for the two different initial conditions, GBW and MV, are presented in Table 1. A partial comparison between the experimental data [1–16] and the results of the fit for $F_2(x, Q^2)$ is shown in Fig. 2.

Initial condition	σ_0 (mb)	Q_{s0}^2 (GeV ²)	C^2	γ	$\chi^2/\text{d.o.f.}$
GBW	31.59	0.24	5.3	1 (fixed)	916.3/844=1.086
MV	32.77	0.15	6.5	1.13	906.0/843=1.075

Table 1: Values of the fitting parameters from the fit to $F_2(x, Q^2)$ data from [1–16] with $x \leq 10^{-2}$ and for all available values of Q^2 , $0.045 \text{ GeV}^2 \leq Q^2 \leq 800 \text{ GeV}^2$.

On the other hand, $F_L(x, Q^2)$ offers an additional constrain on the gluon distribution and is expected to have more discriminating power on different approaches, particularly in the low- Q^2 region [70]. In Fig. 3 we show a comparison between experimental data [17, 18] and our predictions for $F_L(x, Q^2)$.

Several comments are in order. First, the two different initial conditions yield very good fits to F_2 -data, with $\chi^2/\text{d.o.f.} \sim 1$, and almost identical results for F_L .

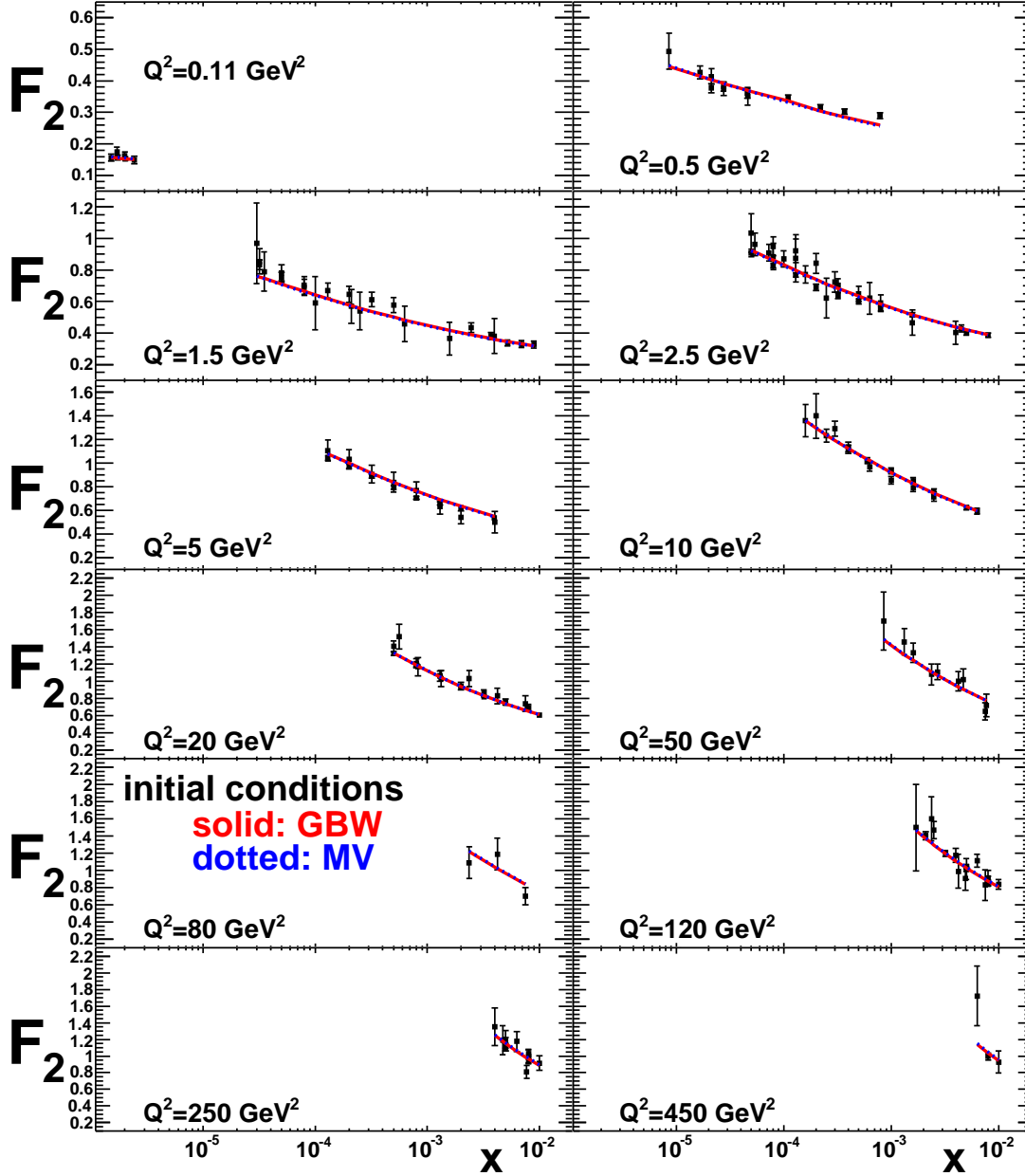


Figure 2: Comparison between a selection of experimental data [1–16] and the results from the fit for $F_2(x, Q^2)$. Solid red lines correspond to GBW i.c., and dotted blue ones to MV i.c. The error bars correspond to statistical and systematic errors added in quadrature.

As remarked in the previous Section the main difference between the two initial conditions is their behavior at small r . In principle this difference is large, but the fact that the values of γ resulting from the fit are different for the different initial conditions, should compensate it in a limited region of r . We thus conclude that the kinematical coverage of the existing experimental data on F_2 (and F_L) is too small

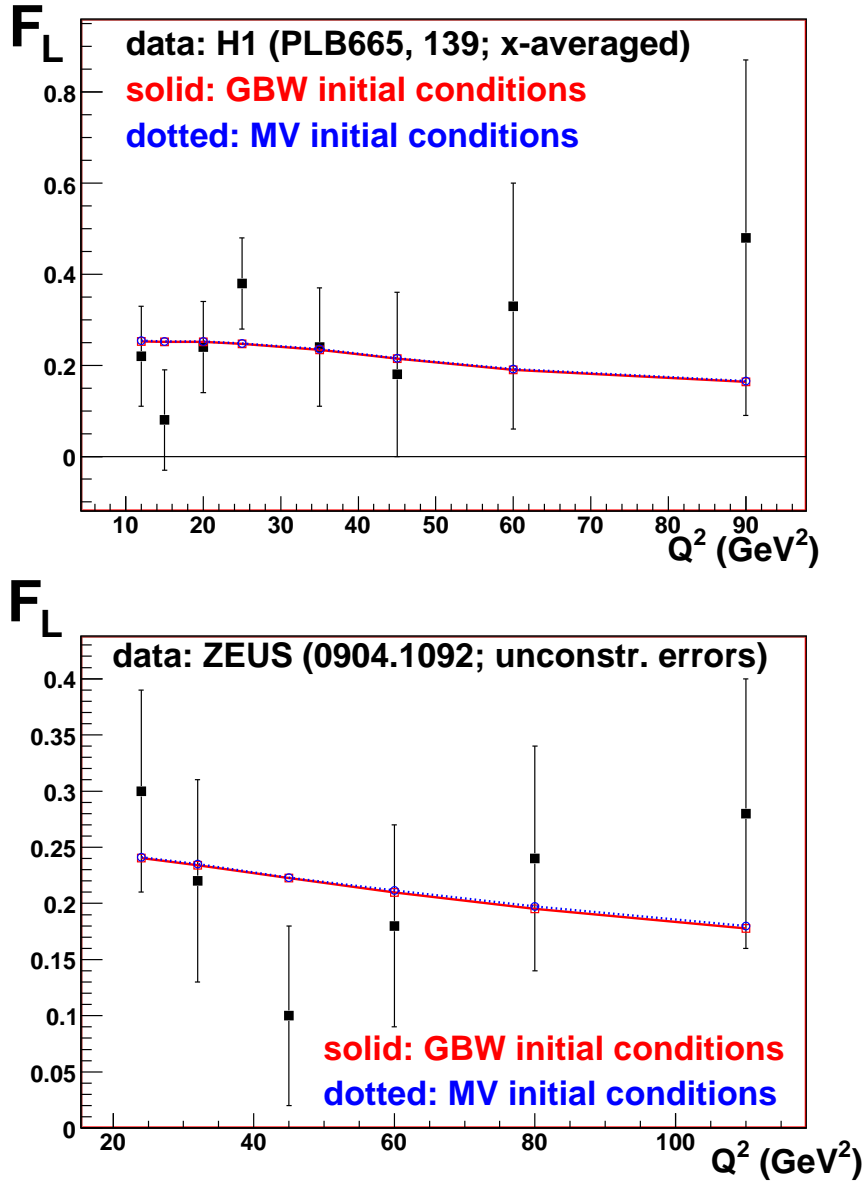


Figure 3: Comparison between experimental data from the H1 [17] (upper plot) and ZEUS [18] (lower plot) Collaborations and the predictions of our model for $F_L(x, Q^2)$. Red solid lines and open squares correspond to GBW i.c., and blue dotted lines and open circles to MV i.c. The theoretical results have been computed at the same $\langle x \rangle$ as the experimental data, and then joined by straight lines. The error bars correspond to statistical and systematic errors added in quadrature for those data coming from [17], while they correspond to the error quoted for the unconstrained fit for those data coming from [18].

to allow a discrimination of the different UV behaviors of the two employed i.c.

Second, the fits using GBW i.c. and obtained by letting γ vary as a free pa-

parameter, do not show an improvement with respect to those obtained by fixing it to $\gamma = 1$. On the contrary, the fits using MV i.c. do improve by letting γ be a free parameter, which takes a value slightly larger than one, $\gamma = 1.13$.

Third, although the two different fits yield pretty different values of the initial proton saturation scale, this apparent discrepancy is due to the different functional forms for GBW and MV i.c. If we redefine the initial saturation scale for the MV i.c. via the condition $\mathcal{N}^{MV}(r = 1/Q'_{s0,MV}, Y = 0) = 1 - e^{-1/4}$ (see Section 4.3), we will get $Q'^2_{s0,MV} \sim 0.19 \text{ GeV}^2$, which is closer to the GBW result. Therefore we conclude from our study that the saturation scale of the proton, obtained in our fit within the dipole model (considering only three active flavors and translational invariant initial conditions i.e. a proton with a constant profile) at $x = 0.01$, lies in the range

$$0.19 \text{ GeV}^2 < Q'^2_{s0} < 0.25 \text{ GeV}^2.$$

Fourth, the values of σ_0 obtained from the fits are very close to each other. This supports the assumption of translational invariance. Furthermore, the obtained values of $\sigma_0 \simeq 32 \text{ mb}$ correspond, assuming a Gaussian form factor for the proton [62], to a diffractive exponential slope $\sigma_0/(4\pi) \simeq 6.5 \text{ GeV}^{-2}$ in agreement with experimental data [71], see the comments below Eq. (2.4).

Fifth, we have checked that the quality of the fit and the values of the parameters are stable under the restriction of the data range to the region $Q^2 < 50 \text{ GeV}^2$ (which leaves 703 data points for the fit). While in principle the dipole model should be more suitable for the description of structure functions in the region of low and moderate Q^2 , we take this stability as a signal that there is no tension in the fit with the large- Q^2 data.

Finally, the agreement of our predictions for $F_L(x, Q^2)$ with the experimental data [17, 18] is of the same quality as other based on fixed-order NLO and NNLO DGLAP evolution, see the comparison in [17, 18]. As discussed in [70], data at smaller Q^2 may offer the possibility of discriminating different approaches.

4.2 Predictions for future experimental programs

Besides available experimental data, the experimental programmes at the LHC will test [19, 58, 72] our understanding of the small- x behavior of the nucleon structure. There are also proposals of future lepton-hadron colliders [56, 57] in which new measurements of structure functions at smaller x would be performed. Further, the physics of high-energy cosmic rays is expected to be influenced by small- x phenomena [59, 60]. Therefore, we find it worth to show in Fig. 4 our predictions for F_2 and F_L in a broad, yet experimentally unexplored region of x and Q^2 .

Two facts should be highlighted. First, the striking agreement of the predictions –which makes them more reliable– from both initial conditions. Second, that at large Q^2 and small x the effect of saturation, namely the flattening of the structure

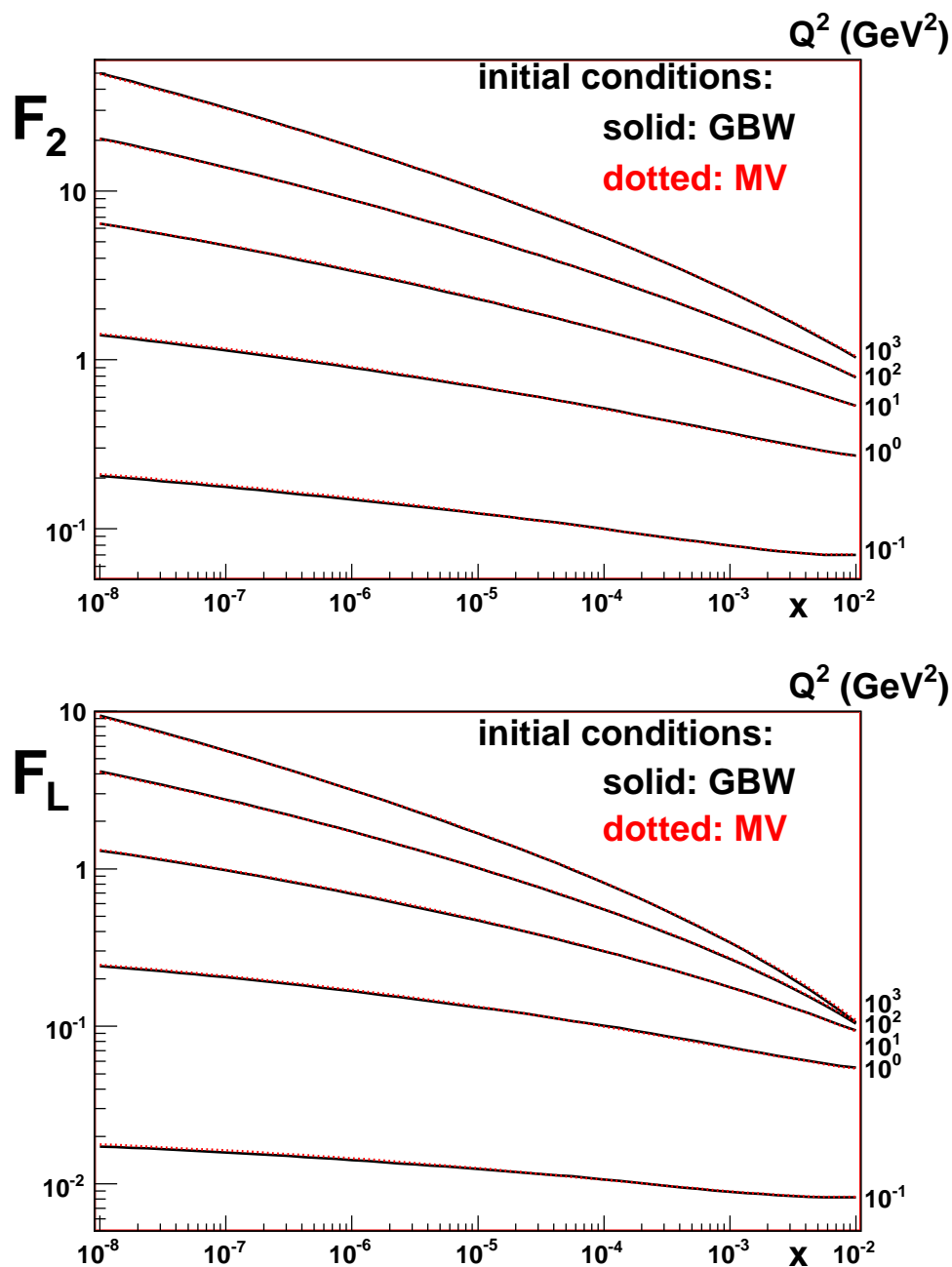


Figure 4: Predictions for $F_2(x, Q^2)$ (top) and $F_L(x, Q^2)$ (bottom) versus x , for $10^{-8} \leq x \leq 10^{-2}$ and $Q^2 = 10^{-1}, 1, 10, 10^2, 10^3$ GeV² (lines from bottom to top). Solid black lines show the results obtained with GBW i.c., and dotted red lines those obtained with MV i.c.

function, is more apparent in F_L than in F_2 . This fact stresses, in our view, the importance of F_L measurements to distinguish different scenarios for the small- x dynamics: fixed order perturbative QCD, resummation schemes or saturation models

[70].

4.3 Parametrizations of the dipole-proton scattering amplitude

With all the uncertainties associated to the initial condition for the evolution fixed by the fit to F_2 presented in the previous sections, we can now evolve the proton-dipole scattering amplitude to much smaller values of x . Such extrapolation is completely driven by small- x evolution including running coupling corrections and can be used to calculate several different observables relevant for the LHC and cosmic ray physics. We have performed the evolution down to $x = 10^{-12}$. The resulting proton-dipole scattering amplitude is plotted in Fig. 5 for three values of x ($x = 10^{-2}, 5 \cdot 10^{-6}$ and $5 \cdot 10^{-9}$) both for MV and GBW i.c. and has been made public through simple fortran routines in [61]. From the solutions of the evolution in Fig. 5 we can extract the proton saturation scale $Q_s(x)$ through the condition

$$\mathcal{N}(r = 1/Q_s(x), x) = \kappa \sim \mathcal{O}(1). \quad (4.1)$$

It is important to note that the values of $Q_s(x)$ presented in Fig. 6 are dependent on the choice of κ in Eq. (4.1). Following the original GBW prescription we take

$$\kappa = 1 - \exp[-1/4] \sim 0.22. \quad (4.2)$$

Different choices of κ can affect the numerical value of $Q_s(x)$ by a factor $\sim 2 \div 3$. Keeping in mind such ambiguity in its extraction from the numerical solutions of the evolution equation, we can estimate the value of the proton saturation scale at LHC energies. Using $2 \rightarrow 1$ kinematics to compute the smallest value of Bjorken- x probed in proton-proton collisions, $x = (2M/\sqrt{s})e^{-y}$, where M is the invariant mass of the produced system (one hadron, dileptons,...), $\sqrt{s} = 14$ TeV is the collision energy and y the rapidity of the produced particle, we get (fixing $M = 1$ GeV) that the saturation scale of the backward-moving proton at the LHC at rapidities $y = 0, 3$ and 6 is $Q_s^2 \simeq 0.55 \div 0.7, 1.3 \div 1.7$ and $3 \div 4$ GeV² respectively. Such values are large enough to suggest that saturation effects in proton-proton collisions at the LHC may be detectable, specially at forward rapidities.

5. Conclusions

We presented a new approach towards a systematic quantification of parton distributions at small- x directly in terms of non-linear QCD evolution equations. This approach has become feasible thanks to the recent calculation of the running coupling corrections to the BK equation. In this work we performed a global fit to the available experimental data for $F_2(x, Q^2)$ measured in electron-proton scattering for $x \leq 10^{-2}$ and all values of Q^2 . The calculation of the structure functions F_2 and F_L is done within the dipole model under the translational invariant approximation

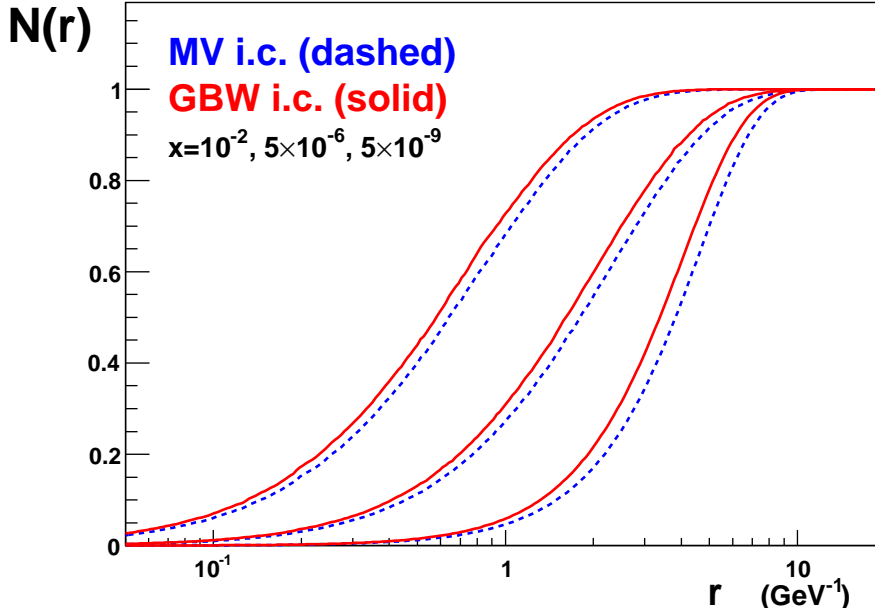


Figure 5: Dipole scattering amplitude obtained from the fits for the two different initial conditions, MV (dashed blue) and GBW (solid red) at $x = 10^{-2}$, $5 \cdot 10^{-6}$ and $5 \cdot 10^{-9}$ (from right to left).

and considering just three active flavors. The main novelty of this work with respect to previous phenomenological analyses is the direct use of the running coupling BK equation to describe the small- x dependence of the structure functions. We find a very good agreement with experimental data with only three (four) free parameters using GBW (MV) initial conditions for the evolution. Available data on F_L , not included in the fit, are also well described. We present predictions for both F_2 and F_L in the kinematic regime relevant for future accelerators and ultra high-energy cosmic rays. We also provide the evolved proton-dipole scattering amplitude down to values of $x = 10^{-12}$ through a simple computer code for public use [61]. Further extension of this work to nuclear targets and hadronic and nuclear collisions is under way.

In conclusion, we find that the recent progress in our knowledge of non-linear small- x evolution brings us to an unprecedented level of precision allowing for a direct comparison with experimental data. This provides a solid theoretical extrapolation of parton densities towards yet empirically unexplored kinematic regions.

Acknowledgments

We would like to thank Daniele Binosi for informative and helpful discussions, Paul Newman for information on the experimental data for F_L , and Mário Santos and the

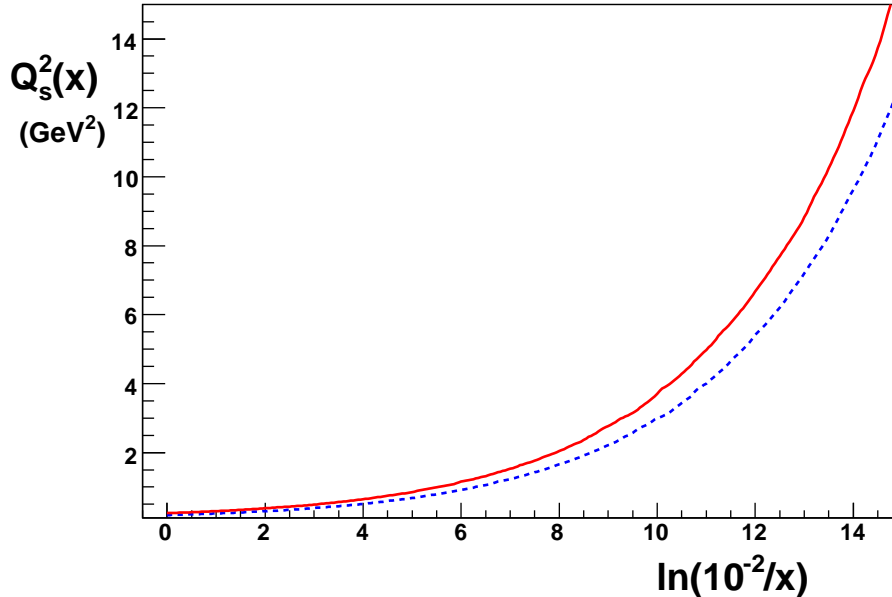


Figure 6: Proton saturation scale, $Q_s^2(x)$ versus $\ln(10^{-2}/x)$ extracted from the solutions in Fig 5 by the condition $\mathcal{N}(r = 1/Q_s(x), x) = 1 - \exp[-1/4]$. The labeling follows the one in Fig. 5.

Observational Cosmology group at CENTRA-IST for their generosity with computing time. This work has been supported by Ministerio de Ciencia e Innovación of Spain under projects FPA2005-01963, FPA2008-01177 and contracts Ramón y Cajal (NA and CAS); by Xunta de Galicia (Consellería de Educación and Consellería de Innovación e Industria – Programa Incite) (NA and CAS); by the Spanish Consolider-Ingenio 2010 Programme CPAN (CSD2007-00042) (NA and CAS); by the European Commission grant PERG02-GA-2007-224770 (CAS); and by Fundação para a Ciência e a Tecnologia of Portugal under project CERN/FP/83593/2008 and contract CIENCIA 2007 (JGM).

References

- [1] **E665** Collaboration, M. R. Adams *et. al.*, *Proton and deuteron structure functions in muon scattering at 470-GeV*, *Phys. Rev.* **D54** (1996) 3006–3056.
- [2] **New Muon** Collaboration, M. Arneodo *et. al.*, *Measurement of the proton and deuteron structure functions, $F_2(p)$ and $F_2(d)$, and of the ratio $\sigma(L)/\sigma(T)$* , *Nucl. Phys.* **B483** (1997) 3–43, [[hep-ph/9610231](#)].
- [3] **H1** Collaboration, I. Abt *et. al.*, *Measurement of the proton structure function $F_2(x, Q^{*2})$ in the low x region at HERA*, *Nucl. Phys.* **B407** (1993) 515–538.

- [4] **H1** Collaboration, T. Ahmed *et. al.*, *A Measurement of the proton structure function $f_2(x, Q^{*2})$* , *Nucl. Phys.* **B439** (1995) 471–502, [[hep-ex/9503001](#)].
- [5] **H1** Collaboration, S. Aid *et. al.*, *A Measurement and QCD Analysis of the Proton Structure Function $F_2(x, Q^2)$ at HERA*, *Nucl. Phys.* **B470** (1996) 3–40, [[hep-ex/9603004](#)].
- [6] **H1** Collaboration, C. Adloff *et. al.*, *A measurement of the proton structure function $F_2(x, Q^{*2})$ at low x and low Q^{*2} at HERA*, *Nucl. Phys.* **B497** (1997) 3–30, [[hep-ex/9703012](#)].
- [7] **H1** Collaboration, C. Adloff *et. al.*, *Measurement of neutral and charged current cross-sections in positron proton collisions at large momentum transfer*, *Eur. Phys. J.* **C13** (2000) 609–639, [[hep-ex/9908059](#)].
- [8] **H1** Collaboration, C. Adloff *et. al.*, *Deep-inelastic inclusive $e p$ scattering at low x and a determination of $\alpha(s)$* , *Eur. Phys. J.* **C21** (2001) 33–61, [[hep-ex/0012053](#)].
- [9] **ZEUS** Collaboration, M. Derrick *et. al.*, *Measurement of the proton structure function F_2 in $e p$ scattering at HERA*, *Phys. Lett.* **B316** (1993) 412–426.
- [10] **ZEUS** Collaboration, M. Derrick *et. al.*, *Measurement of the proton structure function F_2 from the 1993 HERA data*, *Z. Phys.* **C65** (1995) 379–398.
- [11] **ZEUS** Collaboration, M. Derrick *et. al.*, *Measurement of the Proton Structure Function F_2 at low x and low Q^2 at HERA*, *Z. Phys.* **C69** (1996) 607–620, [[hep-ex/9510009](#)].
- [12] **ZEUS** Collaboration, M. Derrick *et. al.*, *Measurement of the F_2 structure function in deep inelastic $e+ p$ scattering using 1994 data from the ZEUS detector at HERA*, *Z. Phys.* **C72** (1996) 399–424, [[hep-ex/9607002](#)].
- [13] **ZEUS** Collaboration, J. Breitweg *et. al.*, *Measurement of the proton structure function F_2 and $\sigma_{tot}(\gamma^* p)$ at low Q^{*2} and very low x at HERA*, *Phys. Lett.* **B407** (1997) 432–448, [[hep-ex/9707025](#)].
- [14] **ZEUS** Collaboration, J. Breitweg *et. al.*, *ZEUS results on the measurement and phenomenology of F_2 at low x and low Q^{*2}* , *Eur. Phys. J.* **C7** (1999) 609–630, [[hep-ex/9809005](#)].
- [15] **ZEUS** Collaboration, J. Breitweg *et. al.*, *Measurement of the proton structure function F_2 at very low Q^{*2} at HERA*, *Phys. Lett.* **B487** (2000) 53–73, [[hep-ex/0005018](#)].
- [16] **ZEUS** Collaboration, S. Chekanov *et. al.*, *Measurement of the neutral current cross section and F_2 structure function for deep inelastic $e+ p$ scattering at HERA*, *Eur. Phys. J.* **C21** (2001) 443–471, [[hep-ex/0105090](#)].

- [17] **H1** Collaboration, F. D. Aaron *et. al.*, *Measurement of the Proton Structure Function F_L at Low x* , *Phys. Lett.* **B665** (2008) 139–146, [[arXiv:0805.2809](#)].
- [18] **ZEUS** Collaboration, S. Chekanov *et. al.*, *Measurement of the Longitudinal Proton Structure Function at HERA*, [arXiv:0904.1092](#).
- [19] M. Dittmar *et. al.*, *Parton Distributions*, [arXiv:0901.2504](#).
- [20] J. Jalilian-Marian, A. Kovner, A. Leonidov, and H. Weigert, *The Wilson renormalization group for low x physics: Towards the high density regime*, *Phys. Rev.* **D59** (1999) 014014, [[hep-ph/9706377](#)].
- [21] J. Jalilian-Marian, A. Kovner, and H. Weigert, *The Wilson renormalization group for low x physics: Gluon evolution at finite parton density*, *Phys. Rev.* **D59** (1999) 014015, [[hep-ph/9709432](#)].
- [22] A. Kovner, J. G. Milhano, and H. Weigert, *Relating different approaches to nonlinear QCD evolution at finite gluon density*, *Phys. Rev.* **D62** (2000) 114005, [[hep-ph/0004014](#)].
- [23] H. Weigert, *Unitarity at small Bjorken x* , *Nucl. Phys.* **A703** (2002) 823–860, [[hep-ph/0004044](#)].
- [24] E. Iancu, A. Leonidov, and L. D. McLerran, *Nonlinear gluon evolution in the color glass condensate. I*, *Nucl. Phys.* **A692** (2001) 583–645, [[hep-ph/0011241](#)].
- [25] E. Ferreiro, E. Iancu, A. Leonidov, and L. McLerran, *Nonlinear gluon evolution in the color glass condensate. II*, *Nucl. Phys.* **A703** (2002) 489–538, [[hep-ph/0109115](#)].
- [26] I. Balitsky, *Operator expansion for high-energy scattering*, *Nucl. Phys.* **B463** (1996) 99–160, [[hep-ph/9509348](#)].
- [27] Y. V. Kovchegov, *Small- x F_2 structure function of a nucleus including multiple pomeron exchanges*, *Phys. Rev.* **D60** (1999) 034008, [[hep-ph/9901281](#)].
- [28] K. Golec-Biernat and M. Wüsthoff, *Saturation effects in deep inelastic scattering at low Q^2 and its implications on diffraction*, *Phys. Rev.* **D59** (1999) 014017, [[hep-ph/9807513](#)].
- [29] E. Iancu, K. Itakura, and S. Munier, *Saturation and bflk dynamics in the hera data at small x* , *Phys. Lett.* **B590** (2004) 199–208, [[hep-ph/0310338](#)].
- [30] E. Gotsman, E. Levin, M. Lublinsky and U. Maor, *Towards a new global QCD analysis: Low x DIS data from non-linear evolution*, *Eur. Phys. J.* **C27** (2003) 411, [[hep-ph/0209074](#)].
- [31] J. L. Albacete, N. Armesto, J. G. Milhano, C. A. Salgado, and U. A. Wiedemann, *Nuclear size and rapidity dependence of the saturation scale from QCD evolution and experimental data*, *Eur. Phys. J.* **C43** (2005) 353–360, [[hep-ph/0502167](#)].

- [32] H. Kowalski and D. Teaney, *An impact parameter dipole saturation model*, *Phys. Rev. D* **68** (2003) 114005, [[hep-ph/0304189](#)].
- [33] H. Kowalski, L. Motyka, and G. Watt, *Exclusive diffractive processes at HERA within the dipole picture*, *Phys. Rev. D* **74** (2006) 074016, [[hep-ph/0606272](#)].
- [34] V. P. Goncalves, M. S. Kugeratski, M. V. T. Machado, and F. S. Navarra, *Saturation physics at HERA and RHIC: An unified description*, *Phys. Lett. B* **643** (2006) 273–278, [[hep-ph/0608063](#)].
- [35] K. Rummukainen and H. Weigert, *Universal features of JIMWLK and BK evolution at small x* , *Nucl. Phys. A* **739** (2004) 183–226, [[hep-ph/0309306](#)].
- [36] Y. V. Kovchegov, J. Kuokkanen, K. Rummukainen, and H. Weigert, *Subleading- N_c corrections in non-linear small- x evolution*, *Nucl. Phys. A* **823** (2009) 47–82, [[arXiv:0812.3238](#)].
- [37] N. N. Nikolaev and B. G. Zakharov, *Colour transparency and scaling properties of nuclear shadowing in deep inelastic scattering*, *Z. Phys. C* **49** (1991) 607–618.
- [38] A. H. Mueller, *Small x Behavior and Parton Saturation: A QCD Model*, *Nucl. Phys. B* **335** (1990) 115.
- [39] J. Bartels, K. J. Golec-Biernat, and H. Kowalski, *A modification of the saturation model: DGLAP evolution*, *Phys. Rev. D* **66** (2002) 014001, [[hep-ph/0203258](#)].
- [40] E. Iancu, K. Itakura, and L. McLerran, *Geometric scaling above the saturation scale*, *Nucl. Phys. A* **708** (2002) 327–352, [[hep-ph/0203137](#)].
- [41] A. H. Mueller and D. N. Triantafyllopoulos, *The energy dependence of the saturation momentum*, *Nucl. Phys. B* **640** (2002) 331–350, [[hep-ph/0205167](#)].
- [42] N. Armesto and M. A. Braun, *Parton densities and dipole cross-sections at small x in large nuclei*, *Eur. Phys. J. C* **20** (2001) 517–522, [[hep-ph/0104038](#)].
- [43] M. A. Braun, *Pomeron fan diagrams with an infrared cutoff and running coupling*, *Phys. Lett. B* **576** (2003) 115, [[hep-ph/0308320](#)].
- [44] J. L. Albacete, N. Armesto, J. G. Milhano, C. A. Salgado, and U. A. Wiedemann, *Numerical analysis of the Balitsky-Kovchegov equation with running coupling: Dependence of the saturation scale on nuclear size and rapidity*, *Phys. Rev. D* **71** (2005) 014003, [[hep-ph/0408216](#)].
- [45] G. Chachamis, M. Lublinsky, and A. Sabio Vera, *Higher order effects in non linear evolution from a veto in rapidities*, *Nucl. Phys. A* **748** (2005) 649–663, [[hep-ph/0408333](#)].
- [46] I. I. Balitsky, *Quark Contribution to the Small- x Evolution of Color Dipole*, *Phys. Rev. D* **75** (2007) 014001, [[hep-ph/0609105](#)].

- [47] Y. Kovchegov and H. Weigert, *Triumvirate of Running Couplings in Small- x Evolution*, *Nucl. Phys. A* **784** (2007) 188–226, [[hep-ph/0609090](#)].
- [48] E. Gardi, J. Kuokkanen, K. Rummukainen, and H. Weigert, *Running coupling and power corrections in nonlinear evolution at the high-energy limit*, *Nucl. Phys. A* **784** (2007) 282–340, [[hep-ph/0609087](#)].
- [49] J. L. Albacete and Y. V. Kovchegov, *Solving High Energy Evolution Equation Including Running Coupling Corrections*, *Phys. Rev. D* **75** (2007) 125021, [[arXiv:0704.0612](#)].
- [50] J. L. Albacete, *Particle multiplicities in Lead-Lead collisions at the LHC from non-linear evolution with running coupling*, *Phys. Rev. Lett.* **99** (2007) 262301, [[arXiv:0707.2545](#)].
- [51] J. L. Albacete, N. Armesto, and J. G. Milhano, *$O(\alpha_s^2)$ -corrections to JIMWLK evolution from the classical equations of motion*, *JHEP* **0611** (2006) 074, [[hep-ph/0608095](#)].
- [52] T. Altinoluk, A. Kovner, M. Lublinsky, and J. Peressutti, *QCD Reggeon Field Theory for every day: Pomeron loops included*, *JHEP* **0903** (2009) 109, [[arXiv:0901.2559](#)].
- [53] I. Balitsky and G. A. Chirilli, *Next-to-leading order evolution of color dipoles*, *Phys. Rev. D* **77** (2008) 014019, [[arXiv:0710.4330](#)].
- [54] A. Dumitru, E. Iancu, L. Portugal, G. Soyez and D. N. Triantafyllopoulos, *Pomeron loop and running coupling effects in high energy QCD evolution*, *JHEP* **0708** (2007) 062, [[arXiv:0706.2540](#)].
- [55] H. Weigert, *Running coupling corrections in small- x evolution*, talk given at the 37th Symposium on Multiparticle Dynamics, August 4-7 2007, LBNL, Berkeley, CA; *Small x evolution in the CGC beyond the total cross section: accommodating diffraction and other restrictions on the final state*, talk given at the International Workshop on Diffraction in High-Energy Physics (Diffraction 08), September 9-14 2008, La Londe-les-Maures, France.
- [56] **The Electron Ion Collider Working Group** Collaboration, C. Aidala *et. al.*, *A High Luminosity, High Energy Electron Ion Collider*, <http://web.mit.edu/eicc/>.
- [57] M. Klein *et. al.*, *Prospects for a Large Hadron Electron Collider (LHeC) at the LHC*, EPAC'08, 11th European Particle Accelerator Conference, 23- 27 June 2008, Genoa, Italy.
- [58] N. Armesto (ed.) *et. al.*, *Heavy Ion Collisions at the LHC - Last Call for Predictions*, *J. Phys. G* **35** (2008) 054001, [[arXiv:0711.0974](#)].
- [59] D. d'Enterria, R. Engel, T. McCauley, and T. Pierog, *Cosmic-ray Monte Carlo predictions for forward particle production in p - p , p - Pb , and Pb - Pb collisions at the LHC*, [arXiv:0806.0944](#).

- [60] N. Armesto, C. Merino, G. Parente, and E. Zas, *Charged Current Neutrino Cross Section and Tau Energy Loss at Ultra-High Energies*, *Phys. Rev.* **D77** (2008) 013001, [[arXiv:0709.4461](#)].
- [61] <http://www-fp.usc.es/phenom/rcbk>.
- [62] C. Marquet, *A unified description of diffractive deep inelastic scattering with saturation*, *Phys. Rev.* **D76** (2007) 094017, [[arXiv:0706.2682](#)].
- [63] E. Levin and M. Lublinsky, *Parton densities and saturation scale from non-linear evolution in DIS on nuclei*, *Nucl. Phys.* **A696** (2001) 833, [[arXiv:hep-ph/0104108](#)].
- [64] N. Armesto and M. A. Braun, *Nuclear structure functions and heavy flavor lepton production off the nucleus at small x in perturbative QCD*, *Eur. Phys. J.* **C22** (2001) 351, [[arXiv:hep-ph/0107114](#)].
- [65] B. Z. Kopeliovich, A. Schafer and A. V. Tarasov, *Nonperturbative effects in gluon radiation and photoproduction of quark pairs*, *Phys. Rev.* **D62** (2000) 054022, [[arXiv:hep-ph/9908245](#)].
- [66] K. Golec-Biernat, L. Motyka, and A. M. Stasto, *Diffusion into infra-red and unitarization of the BFKL pomeron*, *Phys. Rev.* **D65** (2002) 074037, [[hep-ph/0110325](#)].
- [67] J. M. Cornwall, *Dynamical Mass Generation in Continuum QCD*, *Phys. Rev.* **D26** (1982) 1453.
- [68] A. C. Aguilar, D. Binosi, and J. Papavassiliou, *Gluon and ghost propagators in the Landau gauge: Deriving lattice results from Schwinger-Dyson equations*, *Phys. Rev.* **D78** (2008) 025010, [[arXiv:0802.1870](#)].
- [69] L. D. McLerran and R. Venugopalan, *Boost covariant gluon distributions in large nuclei*, *Phys. Lett.* **B424** (1998) 15–24, [[nucl-th/9705055](#)].
- [70] R. S. Thorne, *The Longitudinal Structure Function at HERA*, [arXiv:0808.1845](#).
- [71] **H1** Collaboration, A. Aktas *et. al.*, *Diffractive deep-inelastic scattering with a leading proton at HERA*, *Eur. Phys. J.* **C48** (2006) 749 [[arXiv:hep-ex/0606003](#)].
- [72] A. Accardi *et. al.*, *Hard probes in heavy ion collisions at the LHC: PDFs, shadowing and p A collisions*, [hep-ph/0308248](#).